Highly polarized all-fiber thulium laser with femtosecond-laser-written fiber Bragg gratings

Christina C. C. Willis,[1] Erik McKee,[1] Pascal Böswetter,[1,2] Alex Sincore,[1] Jens Thomas,[3] Christian Voigtländer,[3] Ria G. Krämer,[3] Joshua D. Bradford,[1] Lawrence Shah,[1] Stefan Nolte,[3] Andreas Tünnermann,[3,4] and Martin Richardson[1,*]

[1] *Townes Laser Institute, CREOL College of Optics and Photonics, University of Central Florida, 4000 Central Florida Boulevard, Orlando, Florida 32816, USA*

[2] *Westsächsische Hochschule Zwickau, Dr.-Friedrichs-Ring 2a, 08056 Zwickau, Germany*

[3] *Institute of Applied Physics, Friedrich-Schiller-University, Albert-Einstein-Str. 15, 07745 Jena, Germany*

[4] *Fraunhofer Institute for Applied Optics and Precision Engineering, Albert-Einstein-Str. 7, 07745 Jena, Germany*

[*] *mcr@creol.ucf.edu*

Abstract: We demonstrate and characterize a highly linearly polarized (18.8 dB) narrow spectral emission (<80pm) from an all-fiber Tm laser utilizing femtosecond-laser-written fiber Bragg gratings. Thermally-dependent anisotropic birefringence is observed in the FBG transmission, the effects of which enable both the generation and elimination of highly linearly polarized output. To our knowledge, this is the first detailed study of such thermal anisotropic birefringence in femtosecond-written FBGs.

OCIS codes: (060.3735) Fiber Bragg gratings; (060.3510) Lasers, fiber; (060.2420) Fibers, polarization-maintaining.

References and links

1. R. J. De Young and N. P. Barnes, "Profiling atmospheric water vapor using a fiber laser LIDAR system," Appl. Opt. **49**(4), 562–567 (2010).
2. N. Simakov, A. Hemming, S. Bennetts, and J. Haub, "Efficient, polarised, gain-switched operation of a Tm-doped fibre laser," Opt. Express **19**(16), 14949–14954 (2011).
3. N. M. Fried and B. R. Matlaga, "Laser/light applications in urology," in *Lasers in Dermatology and Medicine* (Springer, 2012), pp. 561–571.
4. S. D. Jackson, "Cross relaxation and energy transfer upconversion processes relevant to the functioning of 2 μm Tm^{3+}-doped silica fibre lasers," Opt. Commun. **230**(1-3), 197–203 (2004).
5. T. S. McComb, M. Richardson, and M. Bass, "High-power fiber lasers and amplifiers," in *Handbook of Optics: Volume V- Atmospheric Optics, Modulators, Fiber Optics, X-Ray and Neutron Optics* (McGraw-Hill, 2009), pp. 25.1–25.33.
6. T. S. McComb, R. A. Sims, C. C. C. Willis, P. Kadwani, V. Sudesh, L. Shah, and M. Richardson, "High-power widely tunable thulium fiber lasers," Appl. Opt. **49**(32), 6236–6242 (2010).
7. A. Tünnermann, T. Schreiber, F. Roeser, A. Liem, S. Hoefer, H. Zellmer, S. Nolte, and J. Limpert, "The renaissance and bright future of fibre lasers," J. Phys. B **38**(9), S681–S693 (2005).
8. D. J. Richardson, J. Nilsson, and W. A. Clarkson, "High power fiber lasers: current status and future perspectives," J. Opt. Soc. Am. B **27**(11), B63–B92 (2010).
9. C. Lu and Y. Cui, "Fiber Bragg grating spectra in multimode optical fibers," J. Lightwave Technol. **24**(1), 598–604 (2006).
10. G. P. Frith, B. Samson, A. Carter, J. Farroni, and K. Tankala, "High power (110W), high efficiency (55%) monolithic FBG-based fiber laser operating at 2 μm," Proc. SPIE **6453**, 64532B, 64532B-2 (2007).
11. Y. J. Zhang, B. Q. Yao, S. F. Song, and Y. L. Ju, "All-fiber Tm-doped double-clad fiber laser with multi-mode FBG as cavity," Laser Phys. **19**(5), 1006–1008 (2009).
12. Y. Zhang, W. Wang, S. Song, and Z. Wang, "Ultra-narrow linewidth Tm^{3+}-doped fiber laser based on intra-core fiber Bragg gratings," Laser Phys. Lett. **6**(10), 723–726 (2009).
13. Y. Zhang, W. Wang, R. L. Zhou, S. Song, Y. Tian, and Y. Wang, "Narrow linewidth Tm^{3+}-doped large core fiber laser based on a femtosecond written fiber Bragg grating," Chin. Phys. Lett. **27**(7), 074214 (2010).
14. Z. Zhang, A. J. Boyland, J. K. Sahu, W. A. Clarkson, and M. Ibsen, "High-power single-frequency thulium-doped fiber DBR laser at 1943 nm," IEEE Photon. Technol. Lett. **23**(7), 417–419 (2011).

15. R. A. Sims, Z. A. Roth, C. C. C. Willis, P. Kadwani, T. S. McComb, L. Shah, V. Sudesh, M. Poutous, E. G. Johnson, and M. Richardson, "Spectral narrowing and stabilization of thulium fiber lasers using guided-mode resonance filters," Opt. Lett. **36**(5), 737–739 (2011).
16. O. Andrusyak, V. Smirnov, G. Venus, V. Rotar, and L. Glebov, "Spectral combining and coherent coupling of lasers by volume Bragg gratings," IEEE J. Sel. Top. Quantum Electron. **15**(2), 344–353 (2009).
17. C. Wirth, O. Schmidt, I. Tsybin, T. Schreiber, T. Peschel, F. Brückner, T. Clausnitzer, J. Limpert, R. Eberhardt, A. Tünnermann, M. Gowin, E. ten Have, K. Ludewigt, and M. Jung, "2 kW incoherent beam combining of four narrow-linewidth photonic crystal fiber amplifiers," Opt. Express **17**(3), 1178–1183 (2009).
18. R. Gafsi and M. A. El-Sherif, "Analysis of induced-birefringence effects on fiber Bragg gratings," Opt. Fiber Technol. **6**(3), 299–323 (2000).
19. P. Torres, J. F. Botero-Cadavid, F. J. Velez, C. M. B. Cordeiro, and C. J. S. de Matos, "Spectral response of FBG written in specialty single-mode fibers," AIP Conf. Proc. **1055**, 65–68 (2008).
20. L. J. Li, Y. G. Liu, S. Z. Yuan, and X. Y. Dong, "Study on temperature and stress characteristics of double-clad fiber Bragg gratings," Proc. SPIE **6351**, 63513K, 63513K-5 (2006).
21. L. A. Fernandes, J. R. Grenier, P. R. Herman, J. S. Aitchison, and P. V. S. Marques, "Stress induced birefringence tuning in femtosecond laser fabricated waveguides in fused silica," Opt. Express **20**(22), 24103–24114 (2012).
22. K. Chah, D. Kinet, M. Wuilpart, P. Mégret, and C. Caucheteur, "Femtosecond-laser-induced highly birefringent Bragg gratings in standard optical fiber," Opt. Lett. **38**(4), 594–596 (2013).
23. E. Wikszak, J. Thomas, S. Klingebiel, B. Ortaç, J. Limpert, S. Nolte, and A. Tünnermann, "Linearly polarized ytterbium fiber laser based on intracore femtosecond-written fiber Bragg gratings," Opt. Lett. **32**(18), 2756–2758 (2007).
24. J. Thomas, E. Wikszak, T. Clausnitzer, U. Fuchs, U. Zeitner, S. Nolte, and A. Tünnermann, "Inscription of fiber Bragg gratings with femtosecond pulses using a phase mask scanning technique," App. Phys. A. **86**(2), 153–157 (2006).
25. J. Thomas, C. Voigtländer, R. G. Becker, D. Richter, A. Tünnermann, and S. Nolte, "Femtosecond pulse written fiber gratings: a new avenue to integrated fiber technology," Laser Photon. Rev. **6**(6), 709–723 (2012).
26. J. F. Bayon, M. Douay, P. Bernage, and P. Niay, "Linearly polarized fiber-optic laser," France Telecom, US Patent 5,561,675 (1996).

1. Introduction

Interest in thulium (Tm) fiber lasers stems from their utility in applications such as directed energy, LIDAR, nonlinear mid-IR generation and a number of medical applications [1–3]. Tm:fiber gain media provide broadband emission from ~1.8–2.1 μm, with a high slope efficiency (80% theoretical [4, 5], >65% experimental [6]) when pumped with 790 nm diodes. Fiber lasers as an architecture have diffraction-limited beam quality, relative insensitivity to environmental variation, and efficient cooling due to the high surface-area-to-volume ratio of their structure [7, 8]. The incorporation of fiber Bragg gratings (FBGs) into Tm:fiber lasers enables compact and robust all-fiber systems with controlled and tailored spectral output [9]. All-fiber thulium lasers that incorporate FBGs have been demonstrated in both multimode [10, 11] and single-mode fibers [12], with slope efficiencies as high as 55% [10], narrow linewidths [13] and high levels of polarization [2, 14].

Here we present a thulium all-fiber oscillator which produces highly linearly polarized output at ~2 μm, and a detailed analysis of how the laser's thermal properties affect its output characteristics. The high output polarization is achieved (without any explicitly polarization-selective elements) by independently temperature tuning the FBGs, which are written via femtosecond (fs) laser pulses into panda-type polarization maintaining (PM) fiber. The polarized output of this laser is desirable for applications such as spectral beam combining, where polarized beams are necessary to achieve high combining efficiency [15], or in configurations that employ polarization insensitive elements such that polarization multiplexing can be employed to increase scalability by a factor of two [16, 17].

The observed performance of the laser and a passive examination of the FBGs indicate the presence of an anisotropic thermal dependence of the FBG birefringence. Previously it has been reported that UV recorded FBGs in non-PM fiber show different levels of induced anisotropic birefringence for applied plane stress and strain [18], and that stress applied to FBGs in PM fiber can cause varying levels of coupling between the x and y axes depending upon the angle at which stress is applied [19, 20]. It has also been noted that the structure of fs-written waveguides has a significant effect on the birefringent behavior of said waveguides

[21]. Given these observed effects of stress, strain, and fs-writing on the behavior of birefringence in FBGs, it follows that the strain induced by thermal expansion or contraction in the FBG (in PM fiber) could yield an anisotropic dependence of the birefringence. Another report showed that for FBGs fs-written in standard single mode fiber operating at 1.5 μm there is no appearance of thermally dependent anisotropic birefringent behavior [22], indicating something unique to the recording process and the fiber-type combination used here. This paper provides a detailed study of such anisotropic thermally dependent behavior, and its application to the generation of highly linearly polarized laser output.

2. Fiber Bragg gratings and fabrication

The FBGs used in this study are written in the center of 1-meter long sections of passive panda-type PM fiber with either low reflectivity (LR) or high reflectivity (HR). The fiber used in these experiments has core and cladding diameters of 10 μm and 130 μm respectively (Nufern PM-TDF-10P/130-HE).

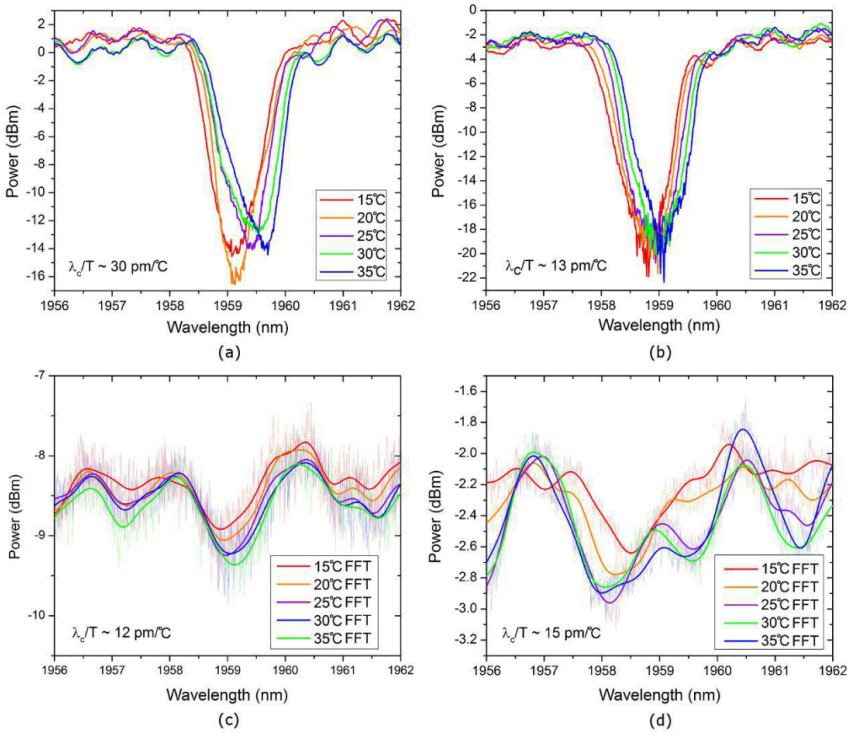

Fig. 1. Spectral transmission of a 2 μm ASE source through each FBG. The HR FBG is shown along the a) slow axis and b) fast axis, and LR FBG is shown along the c) slow axis and d) fast axis.

Traditionally manufactured FBGs use a UV recording process in photosensitive glass to create the Bragg grating [23]. Fs-written FBGs, unlike UV recorded FBGs, do not require the use of photosensitive fiber. Independent of the fs-writing process, FBGs in PM fibers exhibit two reflectivity peaks because of the fiber's birefringence: one peak each for fast and slow axes. The spectral offset of these peaks is determined by the degree of fiber birefringence and the grating period. And due to the nature of the fs-writing process, it is possible for FBGs of the laser-written type to have different level of reflectivity for each axis [23].

The FBGs used here are second order gratings fabricated using 250 μJ pulses projected through a phase mask with a 2.715 μm period [24, 25]. They are written by translating the fiber with respect to illumination source at a velocity of 0.05 mm/min for the HR FBG and 1

mm/min for the LR FBG. The wavelength splitting (spectral offset) for the fast and slow axes is expected to be $\Delta\lambda = 2\Lambda \cdot \Delta n \approx 1.9$ nm (where Λ is the grating period of 2.715 μm and $\Delta n = 3.5 \cdot 10^{-4}$).

The FBGs were characterized passively using an optical spectrum analyzer (Yokogawa AQ6375) to measure the transmission of an isolated broadband ASE source through each FBG. The optical isolation of the ASE source is performed using a fiber-coupled isolator spliced between the ASE source and the FBG. Transmission is measured along each fiber axis as a function of temperature (Fig. 1), and the temperature of the FBG is controlled by mounting it directly on a thermoelectric cooling device (TEC).

The reflectivity of the LR FBG is <30% and its transmission signal is difficult to isolate from the background noise, so an FFT filter was applied to smooth the data (the data before and after smoothing is shown in Figs. 1(c) and 1(d)). The modulation noise in the spectrum is associated with the fiber-coupled isolator placed between the ASE source and the FBG, and is present in both the HR and LR FBG measurements. However, the signal-to-noise ratio is lower in the measurement of the LR FBG, therefore necessitating the FFT smoothing.

Considering Fig. 1, a red-shift in the reflectivity is evident for both the axes of the HR FBG, which changes at a rate of 30 pm/°C along the slow axis and 13 pm/°C along the fast axis. The differing rates of change in reflectivity with temperature indicate the birefringence in the core is temperature dependent. The LR FBG showed a red shift of 12 pm/°C along the slow axis, but exhibited a *blue shift* of 15 pm/°C along the fast axis.

Due to the different rates of change in spectral reflectivity, the separation between the resonances along fast and slow axes for the HR FBG increased from 270 pm at 15 °C to 600 pm at 35 °C, and for the LR FBG increased from 800 pm at 15 °C to 1.130 nm at 35 °C. All of these values are significantly smaller than the a priori estimated spectral separation of 1.9 nm.

3. Laser configuration and experimental set up

The laser architecture is all-fiber, with the pump diode spliced directly to the cavity formed by the FBGs (Fig. 2(a)). The pump diode is fiber coupled and has a maximum output of 35 W at 790 nm (DILAS Diode Laser, Inc.). Its output is spliced to the 1 m passive fiber containing the HR FBG, where the portion containing the FBG is mounted directly on a TEC. The other end of the HR FBG fiber is spliced to a 2 m section of PM active (Tm-doped) fiber with the same dimensions and characteristics as the passive fiber.

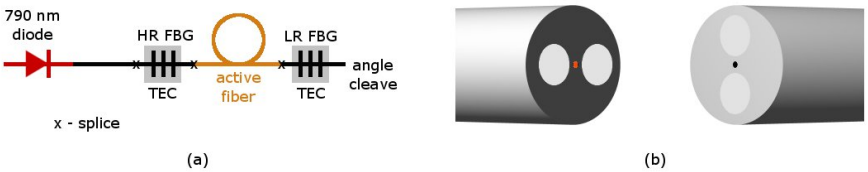

Fig. 2. a) Diagram of the all-fiber laser design, and b) 90° rotated splice between active fiber and LR FBG.

The opposite end of the active fiber is then spliced to the passive fiber containing the LR FBG. A 90° axial rotation is introduced between the active fiber and the fiber of the LR FBG such that their stress rods are oriented orthogonally with respect to each other (Fig. 2(b)). The 90° axial rotation physically aligns the slow axis of the HR FBG to the fast axis of the LR FBG, and the fast axis of the HR FBG to the slow axis of the LR FBG, such that the laser wavelength is determined by the overlap between the spectral reflectivities of the physically aligned (paired) axes [26]. The LR FBG is also mounted on a TEC, and the output end of the passive fiber containing the LR FBG is angle cleaved to prevent parasitic lasing. The active

fiber is wrapped on an 11 cm diameter mandrel that is water-cooled to 13 °C. The temperature of each FBG is controlled independently in steps of 2.5 °C from 15 to 35 °C.

The output light is collimated and transmitted through a dichroic mirror to filter out the remaining pump light, after which the total signal power is measured. The light is then passed through a half-wave plate in a rotation mount, and a polarizing beam cube (PBC). The degree of polarization is measured by taking the ratio of the maximum and minimum power transmitted through the PBC, and spectral measurements are taken at the same point using the optical spectrum analyzer. Spectrum and polarization are measured for all temperature permutations at a set pump power.

4. Laser performance and characterization

The laser had a slope efficiency of 42.4% (Fig. 3(a)), demonstrating a small level of pump cross-relaxation [6]. In the case where the polarization is highest (HR FBG at 15 °C, LR FBG at 17.5 °C), the spectral width of the output is <80 pm FWHM at 1958.3 nm (Fig. 3(b)). The polarization and output wavelength of the system are measured as the temperatures of the FBGs are adjusted. In most temperature permutations, the laser had a highly linearly polarized output with an average polarization of 14.7 dB and a peak value of 18.8 dB (Fig. 4(a)). However, in the range where the HR FBG temperature is minimum (15 °C) and the LR FBG temperature is close to maximum (32.5 °C), the polarization is reduced to a minimum value of 1.8 dB, and two peaks separated by 290 pm are visible in the output spectra.

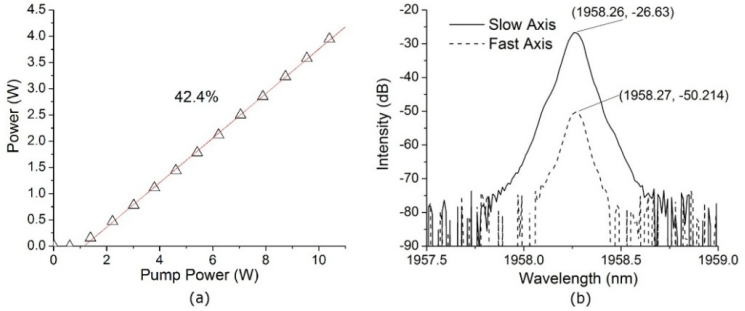

Fig. 3. a) Slope efficiency of the all-fiber laser and b) its spectral output at the point of greatest linear polarization (HR FBG at 15 °C, LR FBG at 17.5 °C).

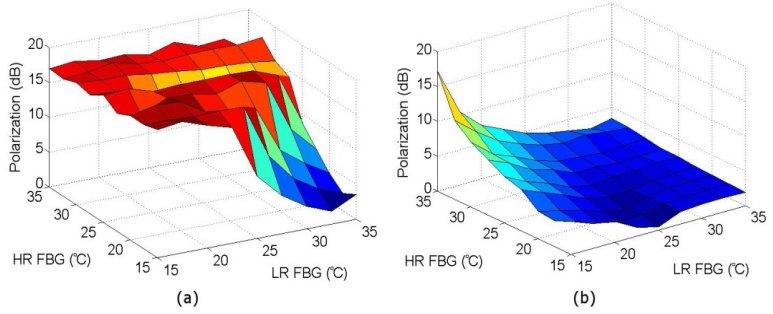

Fig. 4. a) Polarization of the laser containing a 90° rotated splice between active fiber and LR FBG, which has a high linear polarization for most temperature permutations, and b) polarization of the system without a 90° rotated splice, which shows low linear polarization for most temperature permutations.

In contrast, an otherwise identical system without the 90° axial rotation showed a low degree of polarization (Fig. 4(b)) in nearly all temperature permutations (average polarization of 3.7 dB), except when the HR FBG was at 35 °C and the LR FBG was at 15 °C (max polarization of 17.2 dB).

In the system with the 90° axial rotation, temperature tuning of the HR FBG alone (LR FBG held at a fixed temperature) induced a 0.2 pm/°C wavelength redshift for the longer output wavelength, and a 8 pm/°C redshift for the shorter output wavelength (Fig. 5), where the longer wavelength is associated with the HR FBG fast axis/LR FBG slow axis, and the shorter wavelength with the HR FBG slow axis/LR FBG fast axis. Tuning the LR FBG in the same fashion (HR FBG held at a fixed temperature) yields a wavelength dependence of 15 pm/°C redshift for the longer wavelength, and 8 pm/°C redshift for the shorter wavelength. The rate of change with temperature in the laser output wavelengths is different than the rate of change of the peak reflectivity of the FBGs, which was measured passively.

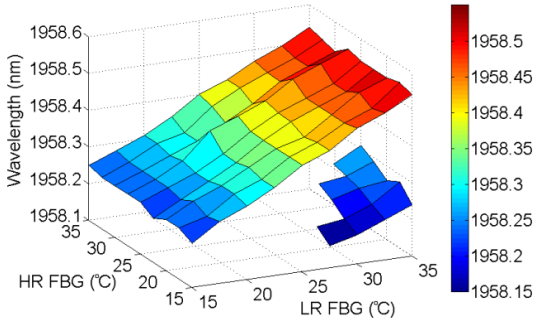

Fig. 5. Wavelengths present in output spectrum at all temperature permutations (fixed pump power), where the upper surface is the longer output wavelength (continuous at all temperatures) and the lower surface is the shorter output wavelength (discontinuous). The shorter wavelength is discontinuous because it is not present in cases of high linear polarization.

5. Analysis of birefringent behavior and temperature tuning results

The FBG characterization and the laser performance together indicate that thermally-dependent birefringence affects the amount of spectral overlap between the physically paired axial reflectivity peaks, and thus determines the laser's output wavelength and polarization. In the case where the stress rods of the HR and LR FBGs are aligned parallel to each other, the slow axis reflectivity of each FBG is paired, and the same with the fast axis. Rotating one of the FBGs along the optic axis by 90° degrees respective to the other (stress rods orthogonal) changes the pairing of the axial reflectivities, slow to fast and fast to slow respectively. The differing rates of change in the peak reflectivity of each FBG, and along each axis, are what generate the different spectral and polarization characteristics in each configuration.

Two specific temperature permutations, one demonstrating high and the other low linear polarization, are shown for the orthogonal laser configuration (Fig. 6). In the case of a high degree of polarization (Figs. 6(a) and 6(b)) the passively measured reflectivity peaks are plotted for the fast and slow axes of the HR and LR FBGs as they are paired in the laser cavity. Comparing the two spectra, the fast axis of the HR FBG and the slow axis of the LR FBG (Fig. 6(b)) have a higher degree of overlap than the other (HR fast to LR slow) axial pairing (Fig. 6(a)). Experimentally, this condition produced a single spectral peak at 1958.30 nm associated with the fast axis of the HR FBG and the slow axis of the LR FBG (Fig. 6(b)). Note that the additional heating of the FBGs under laser operation as compared to the passive case is the most likely cause of the offset between the reflectivity peak overlap and the lasing wavelength that is seen in Fig. 6(b).

In the case with low polarization (Figs. 6(c) and 6(d)) two spectral peaks are observed, one along each axis at 1958.18 and 1958.47 nm. In this case, the reflectivity overlap of the HR fast/LR slow axes has decreased enough that it no longer dominates the other pairing, and therefore allows the second axis to oscillate simultaneously.

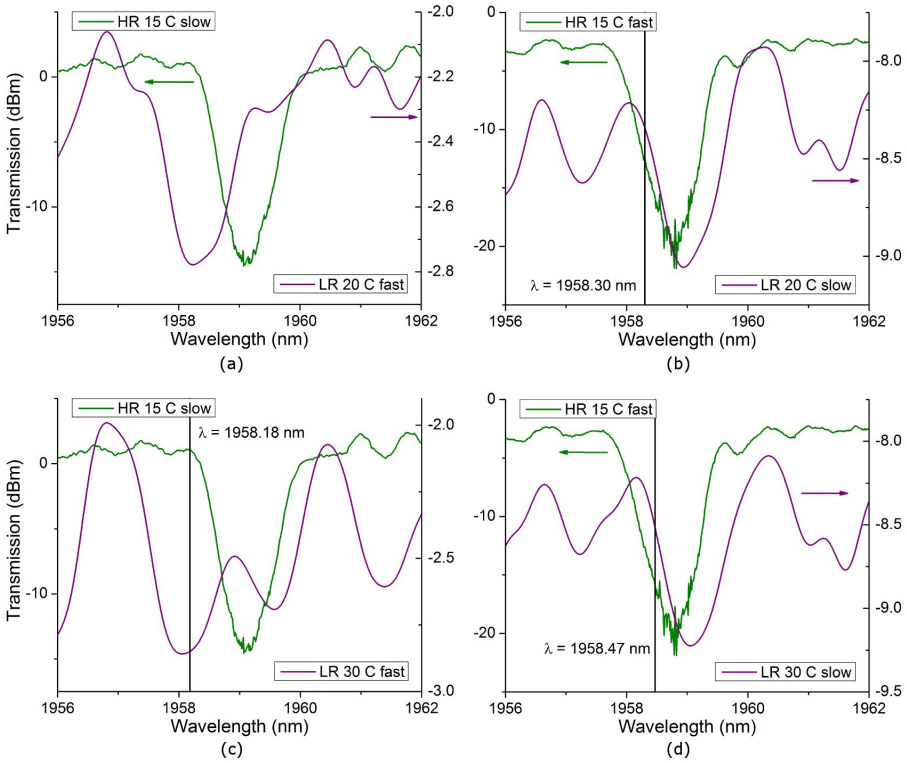

Fig. 6. Spectra showing the overlap of the HR and LR FBG reflectivities for cases of high and low linear polarization. The case of high polarization is shown in a) and b), where the spectral overlap along each optical axis is given for the temperature permutation HR FBG at 15 °C and LR FBG at 20 °C. The case of low linear polarization is shown in c) and d), where the spectral overlap along each optical axis is given for the temperature permutation HR FBG at 15 °C and LR FBG at 30 °C. Note that transmission was measured passively, and in a laser configuration heat loads are different, thus creating an offset between the peaks of the spectral reflectivities and the lasing wavelengths (denoted by vertical black lines).

There is a feature in the transmission of the LR FBG around 1959.9 nm that appears along the fast axis at 30 °C which is not visible at 20 °C (Fig. 1(d)). To establish whether this feature is a result of the modulation noise from the isolator, or if it is a part of the transmission spectrum of the FBG, another case with high polarization where the LR FBG is held at 30 °C is examined (Fig. 7). As can be seen, the pairing of the HR fast axis with the LR slow axis has a very high overlap; however, the overlap between the LR FBG spectral feature at 1959.9 nm and the HR FBG slow axis also appears very high. Since this case shows high level of polarization (only a single spectral peak along the HR FBG fast axis) it would appear that this feature is the result of modulation noise, and not a real spectral feature of the LR FBG.

A similar analysis can be made in the case where all stress rods in the laser system are aligned. The polarization level of this system at different temperature permutations was shown in Fig. 4(b). In this case a high degree of polarization is generated only in one temperature permutation (HR FBG at 35 °C and LR FBG at 15 °C). If there were no anisotropy in the birefringence it would be impossible to vary the degree of polarization because both axes would maintain the same level of spectral overlap at all temperature ranges. It is only the differing temperature tuning rates of the slow and fast axes that allows one axis to develop greater spectral overlap than the other to the point where it dominates and yields a single spectral peak and high linear polarization. An examination of the spectral

overlap of the lone high linear polarization case shows that one axis (fast) has better overlap than the other axis (slow), and the various low polarization cases show a good overlap of both axial pairs. These observations also support our understanding of how high linear polarization is being generated.

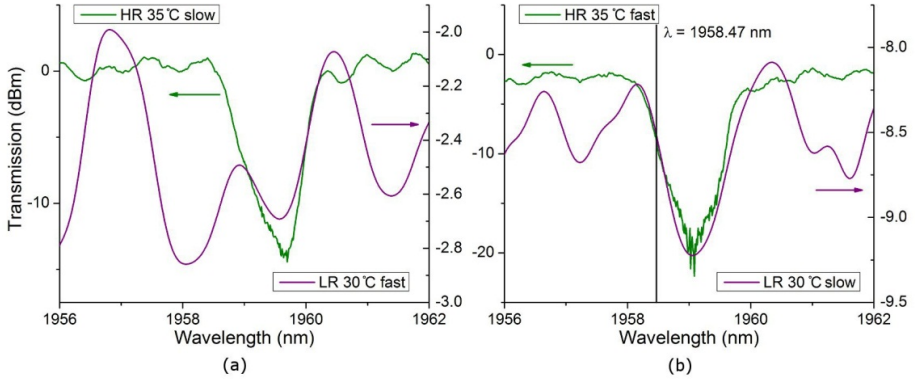

Fig. 7. A case of high polarization (16.16 dB) for orthogonal laser configuration, which can be used to demonstrate that the spectral feature at 1959.9 nm for the LR FBG (at 30 °C) is the result of noise.

Regarding the previously noted blue shift of the LR FBG fast axis, the observed spectral overlaps correspond with a high level of agreement with the levels of polarization measured. This would appear to indicate that the blue shift is a real effect and not a spurious result of the modulation noise. The physical mechanisms that could induce such a behavior are a point of great interest and the subject of further investigation.

6. Conclusion

A laser is demonstrated using fs-laser-written FBGs in which a spectrally narrow laser output (<80 pm) with high degree of polarization (18.8 dB) can be generated without any intra- or extra-cavity polarization selective elements. The high degree of polarization of this system is useful for applications which require a highly polarized all-fiber 2 μm source without additional polarizing elements. Relative axial rotation and temperature tuning of FBGs is used to alter the spectral overlap of the aligned axes, and create a high level of polarization when one pair of axes has a significantly greater spectral overlap than the other pair.

As a result of the analysis of the laser performance and the FBGs under passive conditions, it was determined that there is a thermally anisotropic birefringence in the fs-written FBGs, including the presence of a blue-shift along the fast axis of the LR FBG. Because of this it is possible to generate a significant level of polarization through temperature tuning alone (no axial rotation). This is the first reported analysis of such behavior in fs-written FBGs, and the physical mechanisms of this behavior are the subject of on-going investigation.

Acknowledgments

The US Joint Technology Office (Multiple Research Initiative contract W91NF-05-1-0517 and contract FA9451-10-D-023) and the State of Florida provided the majority of the funding for this research. In addition, Jens Thomas is supported by the Carl-Zeiss-Foundation, Ria G. Krämer is supported by the Abbe School of Photonics, and Christina C. C. Willis wishes to acknowledge the ASEE National Defense Science and Engineering Graduate Fellowship and the Directed Energy Professional Society Fellowship for their support.